In situ Raman study on the impact of configurational entropy on catalytic activity for industrial water oxidation

Chenyang Duan,‡[ab] Hao Zhang,‡[a] Zhiwei Hu,[c] Zhenya Li,[d] Wenjie Bian,[d] Chao Jing,*[ab] Jian-Qiang Wang*[ab] and Linjuan Zhang*[ab]

a.Key Laboratory of Interfacial Physics and Technology, Shanghai Institute of Applied Physics, Chinese Academy of Sciences, Shanghai 201800, P. R. China.

b. University of Chinese Academy of Sciences, Beijing 100049, P. R. China.

c. Max Planck Institute for Chemical Physics of 556 Solids, Dresden 01187, Germany.

d. Shanghai Power Equipment Research Institute Co., Ltd, Shanghai 200240, P. R. China.

E-mail: jingchao@sinap.ac.cn; wangjianqiang@sinap.ac.cn; zhanglinjuan@sinap.ac.cn

‡ These authors contributed equally to the work.

Configurational entropy calculation

We have calculated the configurational entropy (S_{conf}) based on the work of Yeh and co-workers,[1] the configurational entropy is calculated using the formula:

$$S_{\text{conf}} = -R\sum_{i=1}^{n} x_i ln\frac{x_i}{N_i} \quad (1)$$

where:

- x_i is the mole fraction of the i_{th} component in the alloy.
- n is the total number of components in the system.
- R is the gas constant (8.314 J/(mol·K)).

For example, the calculation of S_{conf} of Ni-HEA($Cr_{15}Mn_{15}Fe_{15}Co_{15}Ni_{40}$) would be:

$S_{\text{conf}} = -R \times (x_{Cr} \ln (x_{Cr}) + x_{Mn} \ln (x_{Mn}) + x_{Fe} \ln (x_{Fe}) + x_{Co} \ln (x_{Co}) + x_{Ni} \ln (x_{Ni}))$

$S_{\text{conf}} = -R \times (0.15\times\ln (0.15) + 0.15\times\ln (0.15) + 0.15\times\ln (0.15) + 0.15\times\ln (0.15) + 0.4\times\ln (0.4))$

$S_{\text{conf}} = 1.505\ R$

Sample Preparation. The synthesis process of $Cr_{15}Mn_{15}Fe_{15}Co_{15}Ni_{40}$ is as follows: 26 g of high-entropy alloy powder ($Cr_{20}Mn_{20}Fe_{20}Co_{20}Ni_{20}$, with a particle size less than 20 μm), 12 g of Ni powder (10μm), 2 g of glycerol tristearate, and 12 g of starch were dissolved in a mixed solution composed of 12.5 g of ethanol and 7.5 g of isopropanol. The mixture was then ball-milled for 24 hours to achieve a uniformly mixed slurry.

Subsequently, 4 g of polyvinyl butyral and 1.5 g of dibutyl phthalate were added, and the ball-milling was continued for 48 hours to ensure the uniformity of the mixture. The slurry was then cast using slip casting technology to form a green sheet, which was cut into individual samples. The samples were sintered in a nitrogen atmosphere at a temperature of 1100 °C for 2 hours. During this sintering process, atomic migration between metal particles was induced due to concentration gradients, and all organic components were decomposed, resulting in a fully interconnected porous structure within the material. Similarly, $Cr_{10}Mn_{10}Fe_{10}Co_{10}Ni_{60}$ and $Cr_4Mn_4Fe_4Co_4Ni_{84}$ were synthesized using the same procedure.

Material characterizations. X-ray diffraction (XRD) patterns were obtained using a D8 Advance X'Pert ProSuper diffractometer with Cu Kα radiation (λ = 1.54178 Å). The X-ray Photoelectron Spectroscopy (XPS)measurements were conducted using a ThermoFisher Scientific ESCALAB Xi+ spectrometer, with a monochromatized Al Kα X-ray source (hν= 1486.6 eV) and a pass energy of 30 eV, the binding energy values were referenced and calibrated against the C 1s peak of adventitious carbon at 284.80 eV. Scanning electron microscopy (SEM) images were collected on a LEO 1530VP SEM at 15 kV. Transmission electron microscopy (TEM) and Energy-dispersive X-ray spectroscopy (EDS)

characterizations were performed with a Tecnai G2 F20 S-TWIN transmission electron microscope.

Electrolytic cell. The electrolyzer comprises two stainless steel collectors with flow channels, two Polyphenylene sulfide (PPS) gaskets, and diaphragms. The electrode area for both the cathode and anode is 2 x 2 cm^2. The anode uses Ni-HEA as the catalyst, and the cathode uses Raney Ni as the catalyst. Durability tests are conducted at 20 °C and 50 °C using a potentiostat with a flowing electrolyte of 5 M KOH.

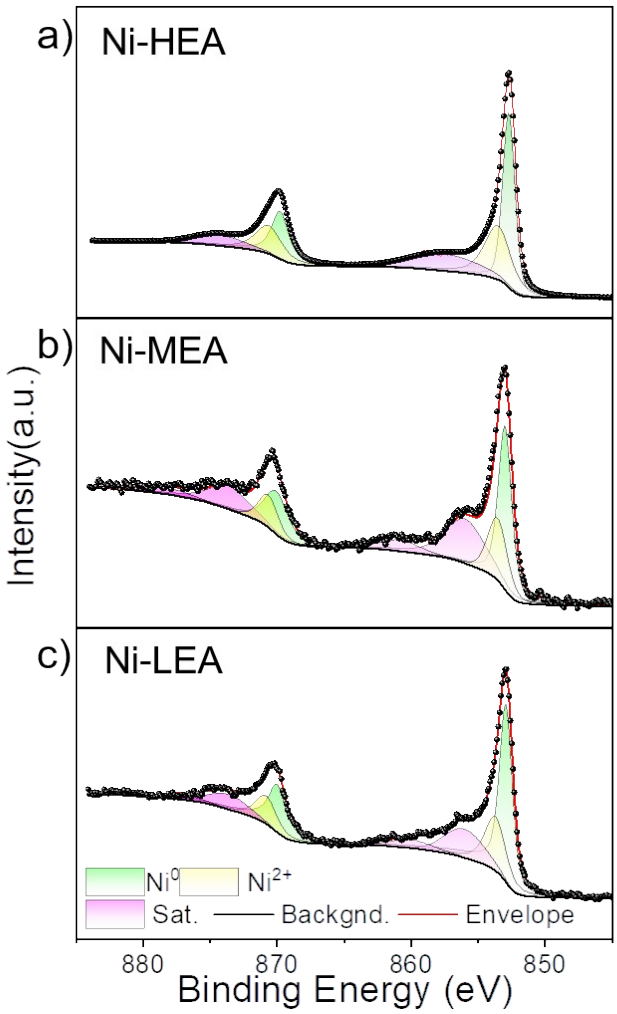

Figure S1 X-ray photoelectron spectroscopy (XPS) analysis of Ni 2p in Ni-HEA **(a)**, Ni-MEA **(b)** and Ni-LEA **(c)** before reaction, respectively.

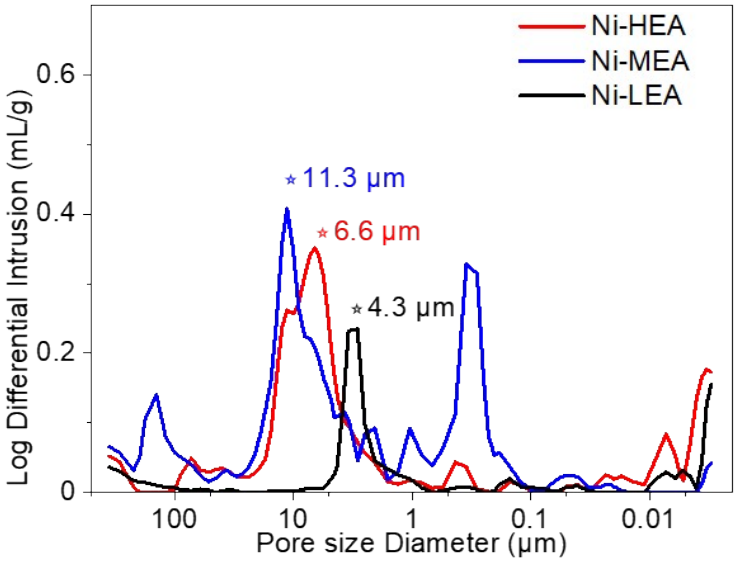

Figure S2 Pore size distribution of Ni-HEA, Ni-MEA and Ni-LEA measured by mercury intrusion porosimetry (MIP).

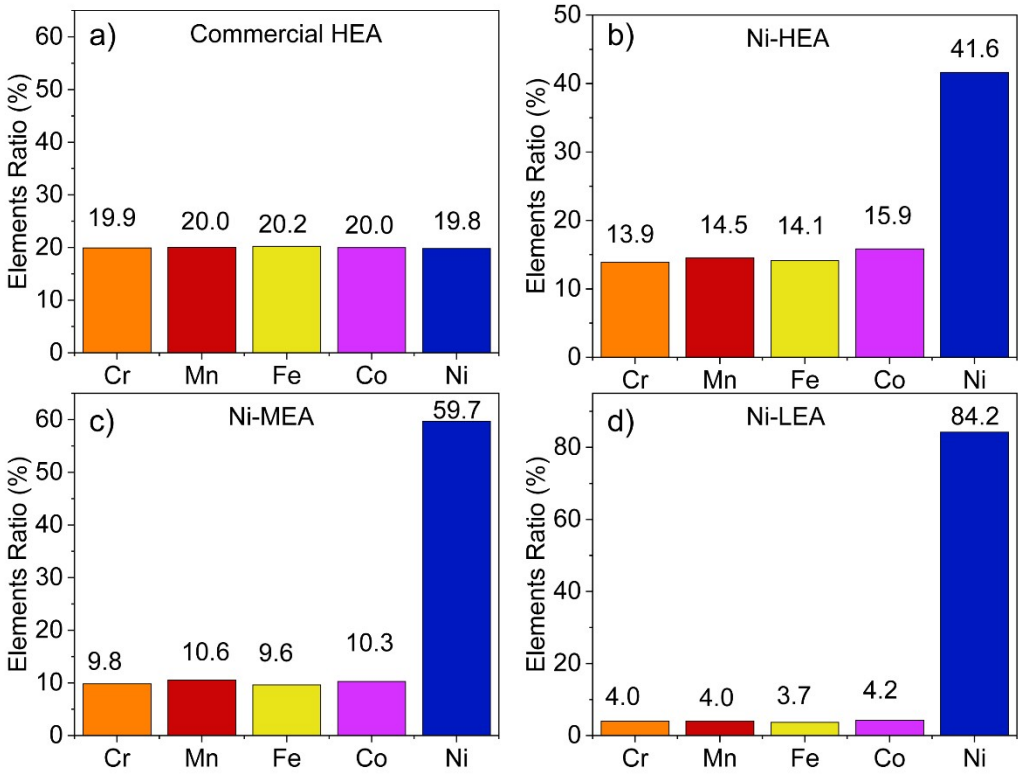

Figure S3 Inductively coupled plasma-mass spectrometry (ICP-MS) results of commercial HEA **(a)**, Ni-HEA **(b)**, Ni-MEA **(c)** and Ni-LEA **(d)**.

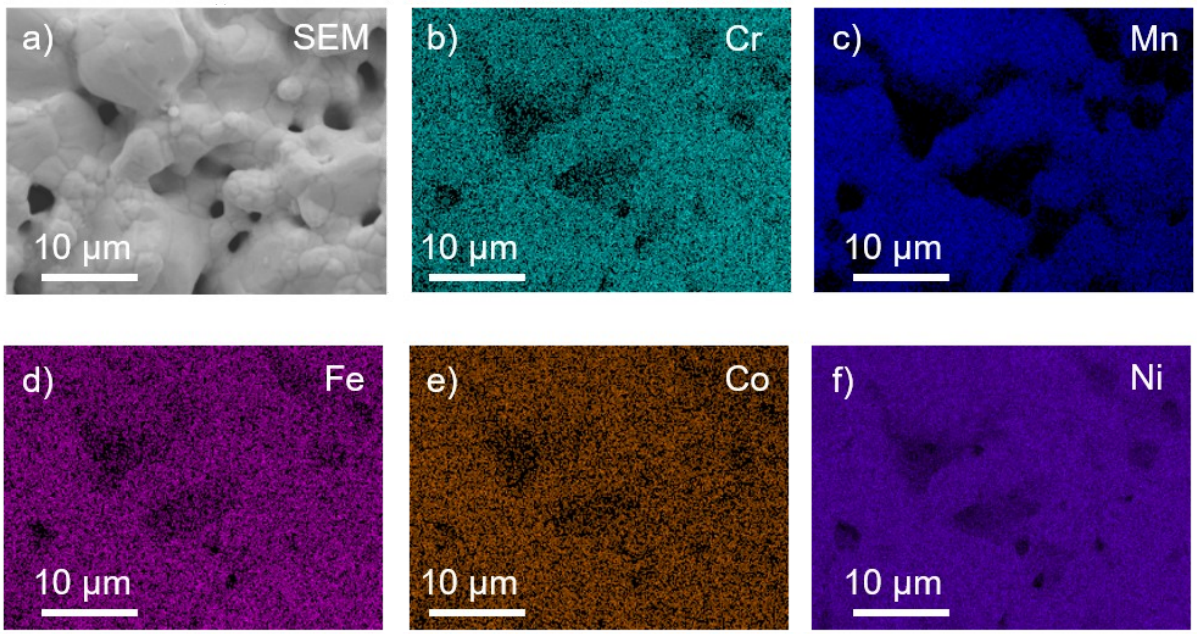

Figure S4 Energy-dispersive X-ray spectroscopy (EDS) elemental mapping of the Ni-HEA.

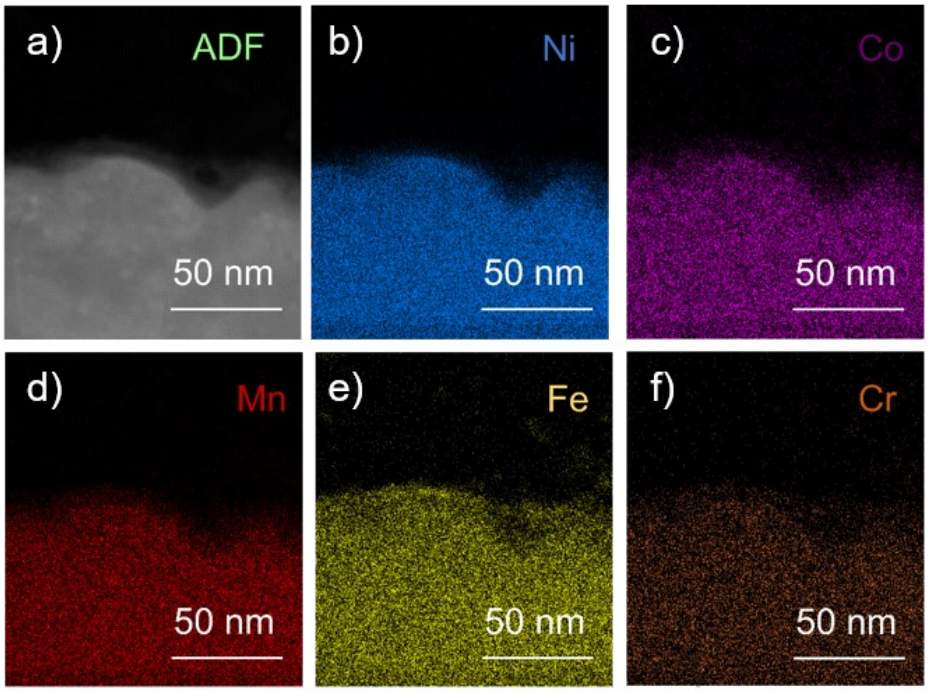

Figure S5 EDS of the surface of Ni-HEA.

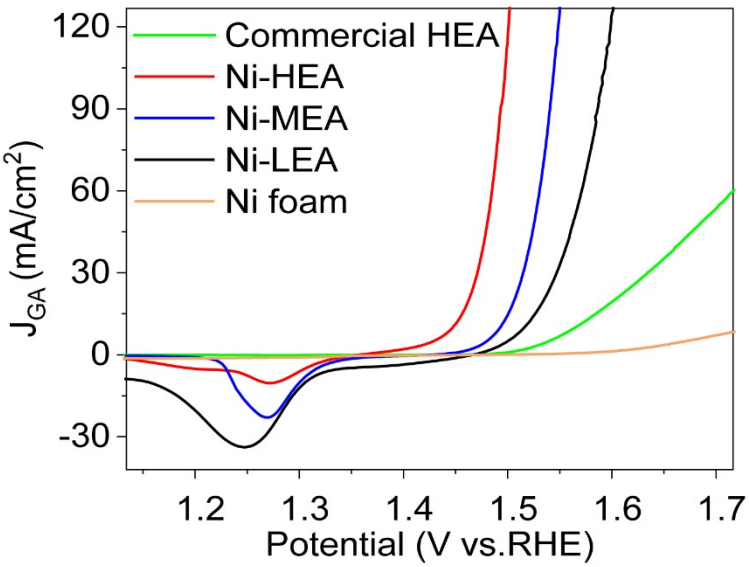

Figure S6 Linear Sweep Voltammetry (LSV) of commercial HEA, Ni-HEA, Ni-MEA and Ni-LEA with 90% iR correction, normalized by the geometric area (GA).

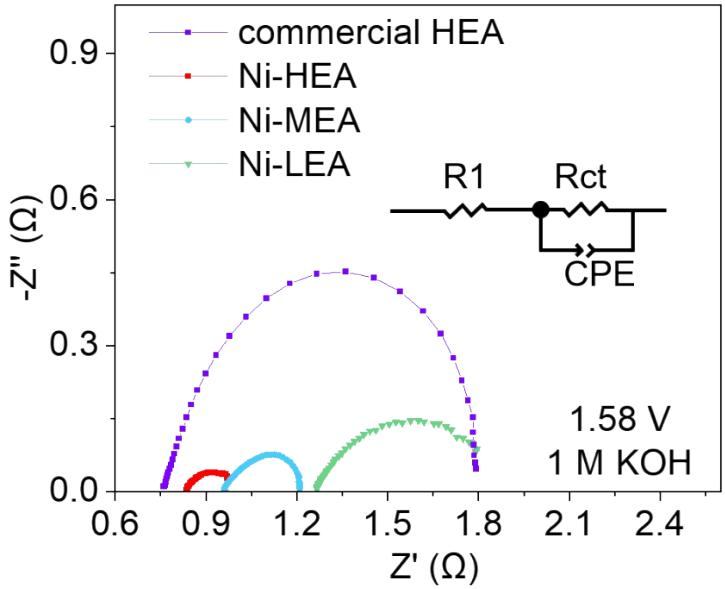

Figure S7 Electrochemical impedance spectroscopy (EIS) of commercial HEA, Ni-HEA, Ni-MEA and Ni-LEA, evaluated at 1.58 V vs. RHE.

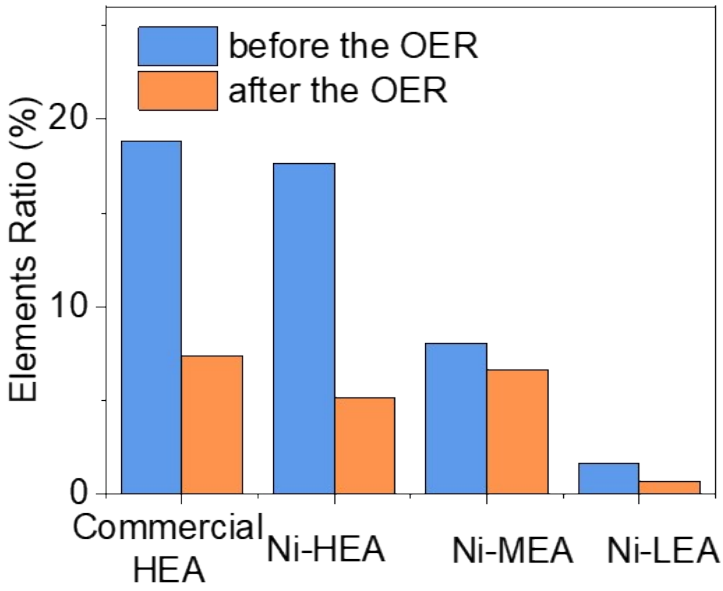

Figure S8 Element proportion of Cr in all samples before and after the OER, measured via EDS.

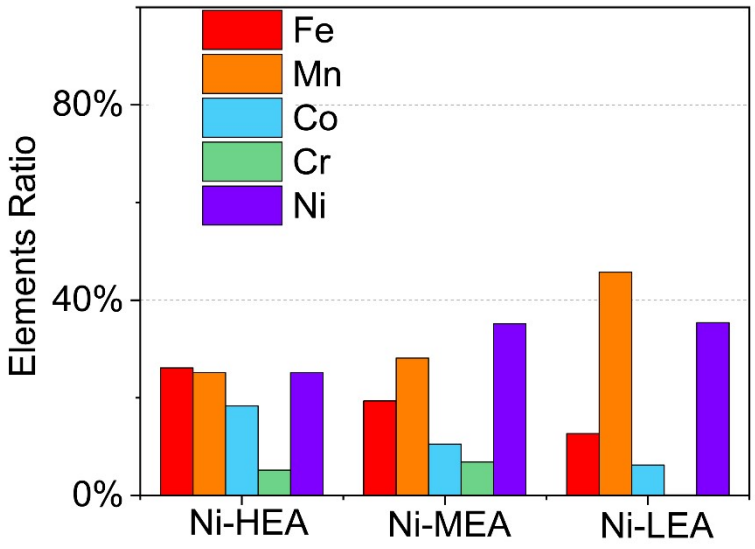

Figure S9 Element proportion of the electrochemical activated surface of Ni-HEA, Ni-MEA and Ni-LEA, measured via XPS.

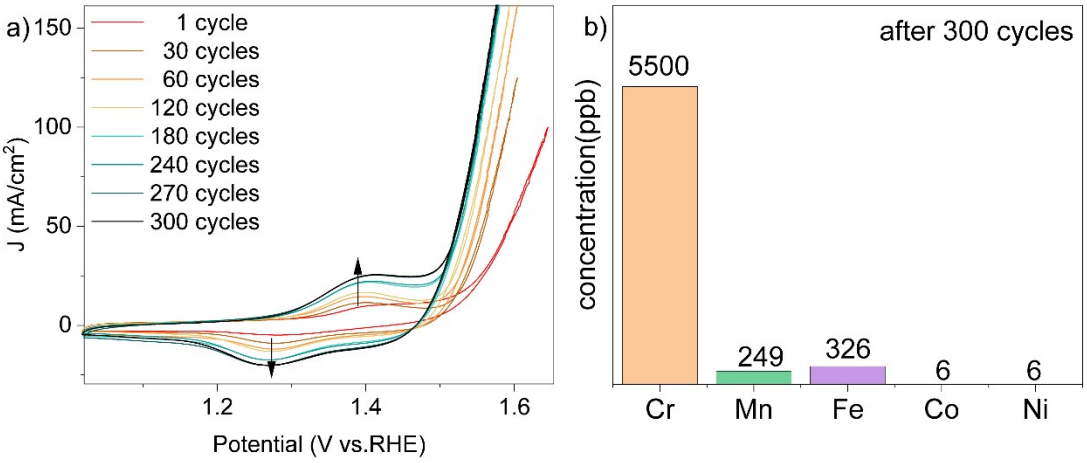

Figure S10 (a) Cyclic voltammetry (CV) curves of Ni-HEA in 1 M KOH solution at a scan rate of 50 mV/s over 300 cycles. **(b)** ICP-MS results of the final solution after 300 CV cycles.

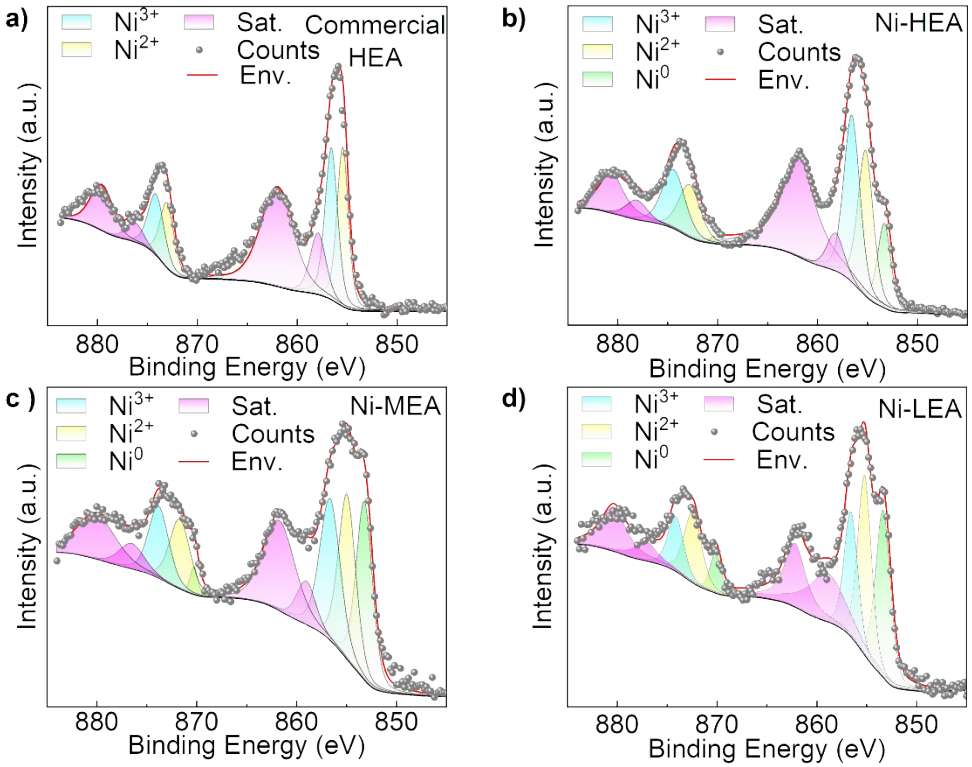

Figure S11. XPS analysis of Ni 2p in commercial HEA **(a)**, Ni-HEA **(b)**, Ni-MEA **(c)**, and Ni-LEA **(d)** after the OER, respectively.

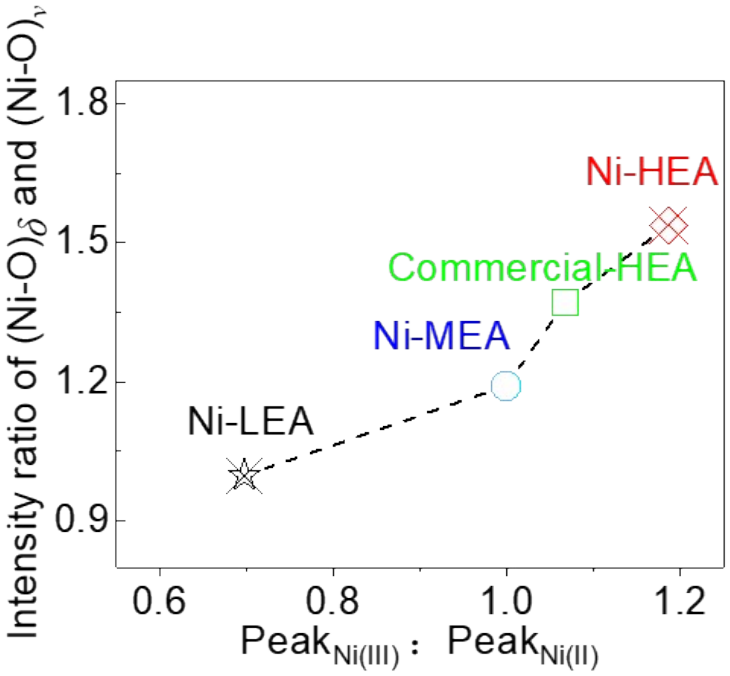

Figure S12 Relationship between the oxidation states of Ni observed in XPS and the I_δ/I_ν observed in Raman spectroscopy at 1.42 V.

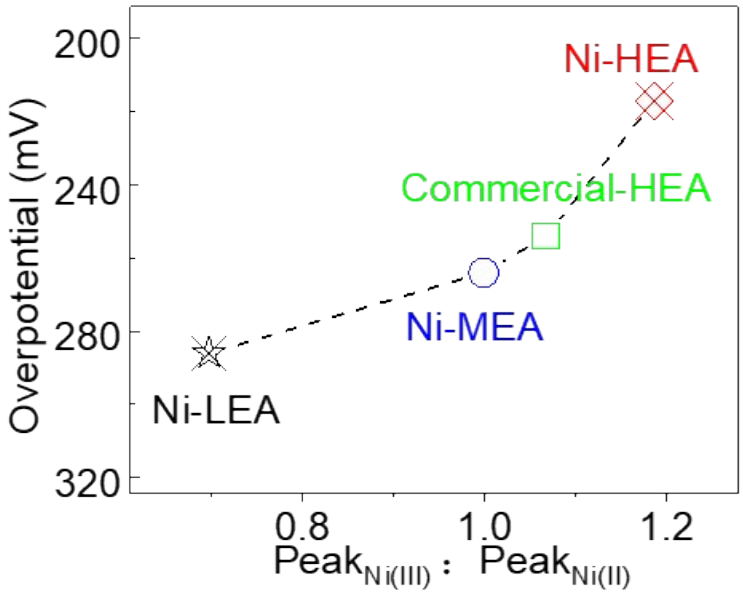

Figure S13 Relationship between the oxidation states of Ni observed in XPS and the overpotential required to achieve a current density of 10 mA/cm².

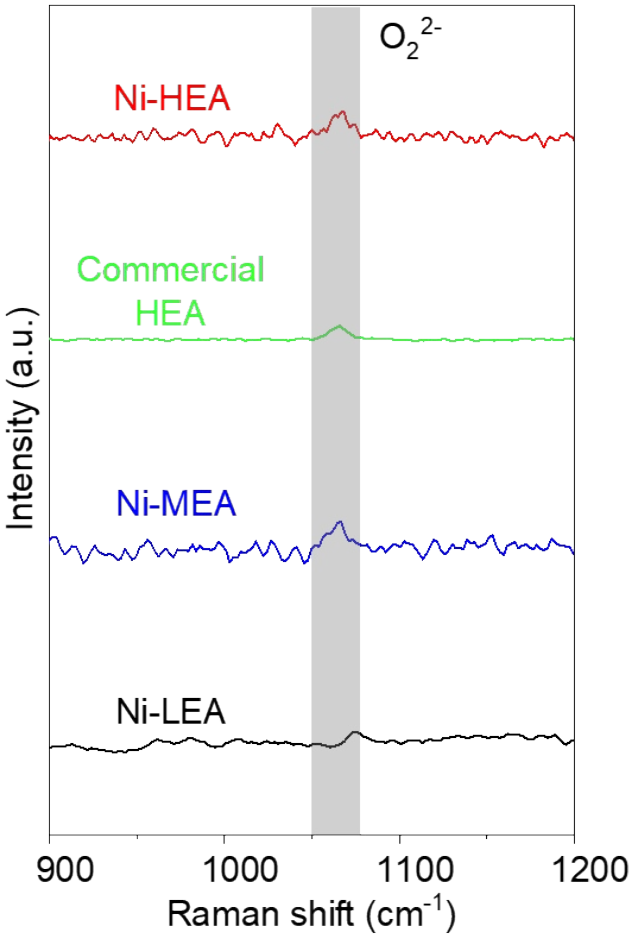

Figure S14 In situ Raman spectra of all samples at 1.42 V in 1 M KOH electrolyte.

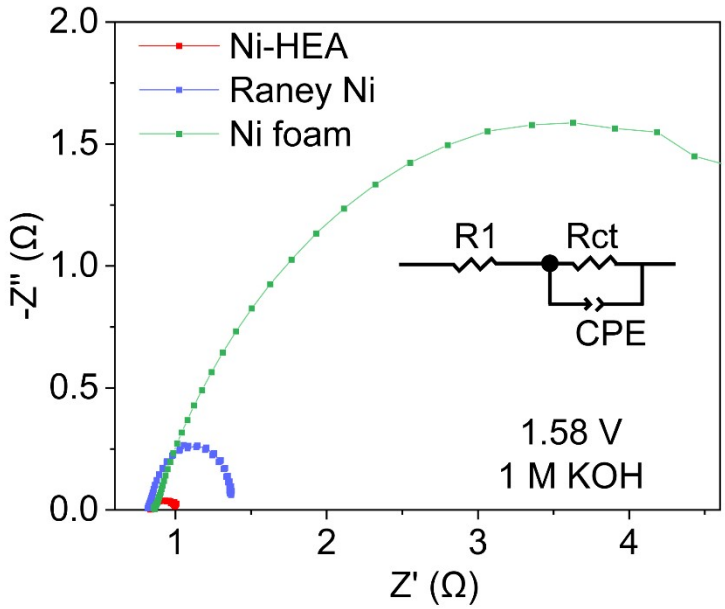

Figure S15 EIS of Ni foam, Raney Ni and Ni-HEA, evaluated at 1.58 V vs. RHE.

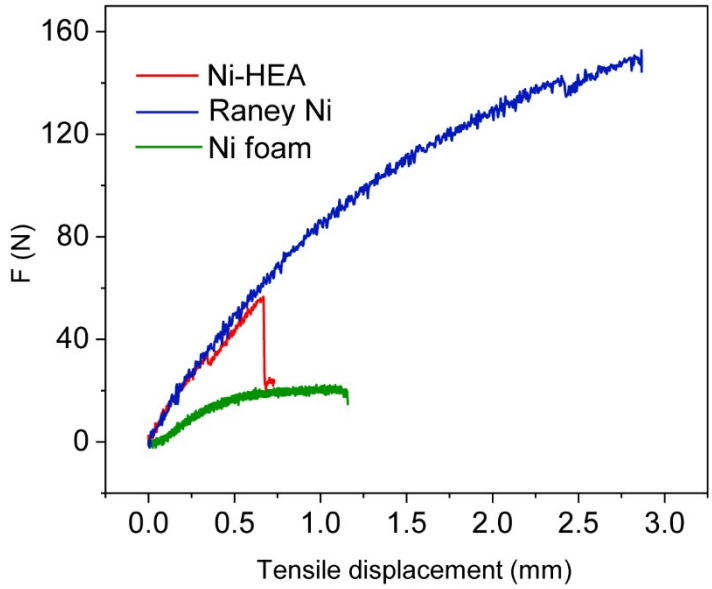

Figure S16 Tensile strength of Ni-HEA, Ni Foam and Raney Ni.

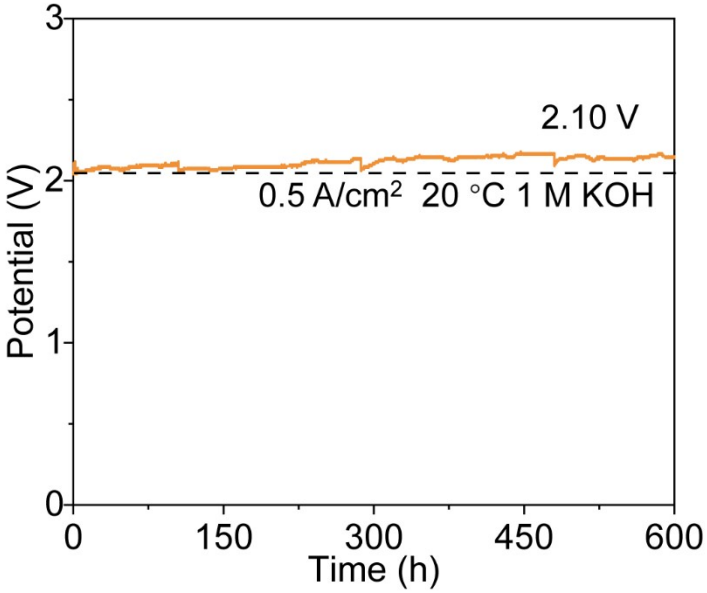

Figure S17 Stability test of Ni-HEA at a constant current density of 0.5 A/cm² in a 5 M KOH solution at 20 °C for 600 hours.

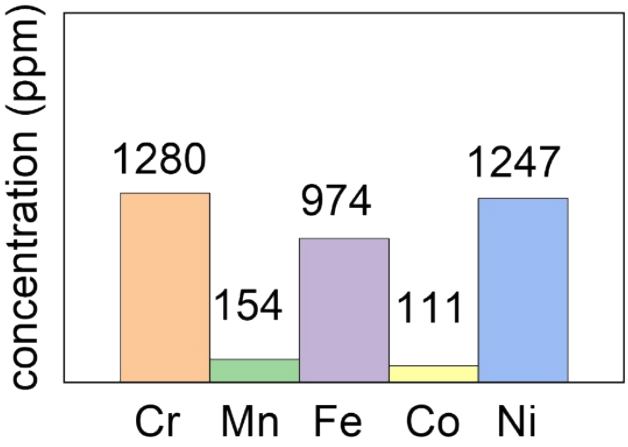

Figure S18 ICP-MS results of the final solution after 200 h stability test under industrial condition.

Table S1. Comparison of the Total pore area and ECSA.

Catalyst	ECSA (mF/cm^2)	Total Pore Area (m^2/g)	Method
Ni-HEA	14.7	42.21	MIP
Ni-MEA	6.9	5.755	MIP
Ni-LEA	12.2	18.87	MIP
commercial HEA	0.45	0.4774	BET

Table S2. Comparison of the catalytic OER performance between this CrMnFeCoNi HEA catalyst and similar catalysts reported in recent literature in alkaline media.

Catalyst	**η@j (mV@mA cm^{-2})**	**Tafel slope (mV dec^{-1})**	**Ref.**
CrMnFeCoNi	**217@10** **266@100**	**46.3**	**This work**
FeCoNiMnCr	**241 @10** **320 @500**	**99.8**	[2]
MnFeCoNiCu	**263@10**	**43**	[3]
np-AlCrCuFeNi	**270@10**	**77.5**	[4]
L5M2Co	**325@10**	**51.2**	[5]
LiNiO2	**315@10**	**53**	[6]
Ir@Co3O4	**280@10**	**73**	[7]
FeCoNi-LDHs	**269@10**	**42.3**	[8]
CoCrRhO	**263@10**	**52.6**	[9]
NiFe-MOF/G	**258@10**	**49**	[10]
IrOx	**255@10**	**48**	[11]
AlNiCoRuMo	**248@10**	**109**	[12]
AlNiCoIrMo	**275@10**	**110.4**	[13]
FeCoNiCrNb	**288@10**	**55.4**	[14]
MnFeCoNi	**325@10**	**51.2**	[15]

References

1. J. W. Yeh, S. K. Chen, S. J. Lin, J. Y. Gan, T. S. Chin, T. T. Shun, C. H. Tsau and S. Y. Chang, *Mater. Sci. Eng. A*, 2004, **6**, 299.
2. J. Hu, T. Guo, X. Zhong, J. Li, Y. Mei, C. Zhang, Y. Feng, M. Sun, L. Meng, Z. Wang, B. Huang, L. Zhang and Z. Wang, *Adv. Mater.*, 2024, **36,** 2310918.
3. K. Huang, B. Zhang, J. Wu, T. Zhang, D. Peng, X. Cao, Z. Zhang, Z. Li and Y. Huang, *J. Mater. Chem. A*, 2020, **8**, 11938.
4. A. K. Ipadeola, A. K. Lebechi, L. Gaolatlhe, A. B. Haruna, M. Chitt, K. Eid, A. M. Abdullah and K. I. Ozoemena, *Electrochem. Commun.*, 2022, **136**, 107207
5. T. X. Nguyen, Y. C. Liao, C. C. Lin, Y. H. Su and J. M. Ting, *Adv. Funct. Mater.*, 2021, **31**, 2101632.
6. H. L. Huang, Y. C. Chang, Y. C. Huang, L. L. Li, A. C. Komarek, L. H. Tjeng, Y. Orikasa, C. W. Pao, T. S. Chan, J. M. Chen, S. C. Haw, J. Zhou, Y. F. Wang, H. J. Lin, C. T. Chen, C. L. Dong, C. Y. Kuo, J. Q. Wang, Z. W. Hu and L. J. Zhang, *Nat. Commun.*, 2023, **14**, 2112.
7. Y. W. Dai, J. Yu, J. Wang, Z. P. Shao, D. Q. Guan, Y. C. Huang and M. Ni, *Adv. Funct. Mater.*, 2022, **32**, 2111989.
8. X. Zhang, F. Yan, X. Ma, C. Zhu, Y. Wang, Y. Xie, S.-L. Chou, Y. Huang and Y. Chen, *Adv. Energy Mater.*, 2021, **11**, 2102141.
9. D. Jin, H. Woo, S. Prabhakaran, Y. Lee, M. H. Kim, D. H. Kim and C. Lee, *Adv. Funct. Mater.*, 2023, **33**, 2301559.
10. Y. Wang, B. Liu, X. Shen, H. Arandiyan, T. Zhao, Y. Li, M. Garbrecht, Z. Su, L. Han, A. Tricoli and C. Zhao, *Adv. Energy Mater.*, 2021, **11**, 2003759.
11. C. Lee, K. Shin, Y. Park, Y. H. Yun, G. Doo, G. H. Jung, M. Kim, W.-C. Cho, C.-H. Kim, H. M. Lee, H. Y. Kim, S. Lee, G. Henkelman and H.-S. Cho, *Adv. Funct. Mater.*, 2023, **33**, 2301557.
12. Z. Jin, J. Lyu, Y.-L. Zhao, H. Li, X. Lin, G. Xie, X. Liu, J.-J. Kai and H.-J. Qiu, *ACS Mater. Lett.*, 2020, **2**, 1698.
13. Z. Jin, J. Lv, H. Jia, W. Liu, H. Li, Z. Chen, X. Lin, G. Xie, X. Liu, S. Sun and H.-J. Qiu, *Small*, 2019, **15**, 1904180.
14. Z. Ding, J. Bian, S. Shuang, X. Liu, Y. Hu, C. Sun and Y. Yang, *Adv. Sustain. Syst.*, 2020, **4**, 1900105.
15. W. Dai, T. Lu and Y. Pan, *J. Power Sources*, 2019, **430**, 104.